Analysis of linear and nonlinear photonic devices using eigenmode expansion

Björn Maes[a,b], Mihai Ibanescu[b], Marin Soljačić[b], John D. Joannopoulos[b], Peter Bienstman[a], Roel Baets[a]

[a]Photonics Research Group, Ghent University, St.-Pietersnieuwstraat 41, 9000 Ghent, Belgium;
[b]Dept. of Physics, Center for Materials Science and Engineering, Research Laboratory of Electronics, Massachusetts Institute of Technology, 77 Massachusetts Avenue, Cambridge 02139, Massachusetts, USA

ABSTRACT

The simulation method known as eigenmode expansion proves to be a versatile approach for modeling microphotonic devices. Originally the tool was developed for high-contrast linear designs. However, it was also extended towards nonlinear effects, such as the Kerr nonlinearity and second-harmonic generation. Here we address recent numerical and theoretical results, obtained or supported by the eigenmode method. In the linear regime, we study high quality cavities, originating from multimode interference through the multipole cancelation mechanism. For the nonlinear regime we present a photonic crystal switching device based on a symmetry breaking instability.

Keywords: Photonics, numerical modeling, micro-cavities, Kerr effect

1. INTRODUCTION

The numerical method of eigenmode expansion is very efficient for a multitude of applications. In this Proceeding we discuss how it applies to the analysis of two different devices. The first application is a linear one: we discuss how to create high-quality cavities using a section of a multimodal waveguide. The second application is nonlinear: we show how two coupled Kerr cavities give rise to the phenomenon of symmetry breaking.

The numerical results in both cases are checked and modeled employing a semi-analytical theory. The use of mode expansion is very important for these theoretical insights, as it immediately gives the amplitudes of the interacting modes. This is in contrast with full-field simulation methods such as finite-difference time-domain (FDTD) or finite element methods.

The manuscript is organized as follows. In the next section we describe the eigenmode algorithm. Both the linear and nonlinear approaches are explained. Then we apply this method to the multimode cavities in a cylindrical geometry. Good agreement with finite-difference time-domain is reached, and a theoretical description is provided. Then, the nonlinear algorithm is applied to coupled photonic crystal resonators. The symmetry breaking phenomena in this system are well described by coupled-mode theory analysis. We close in the concluding section.

2. MODELING METHOD

2.1 Linear devices

In eigenmode expansion a structure is divided into sections that are invariant along a propagation direction. See Fig. 1 for a simple example with three sections. Here, the horizontal direction is the main propagation direction. The field in an invariant section is described as a superposition of modes. These modes and their propagation constants are derived from the transversal index profile. In the end, the field is described by a finite vector of complex amplitudes. This is a much more efficient way than handling the field at each point of a grid.

Further author information: bjorn.maes@ugent.be

Photonics North 2007, edited by John Armitage,
Proc. of SPIE Vol. 6796, 67963B, (2007)
0277-786X/07/$18 · doi: 10.1117/12.778957

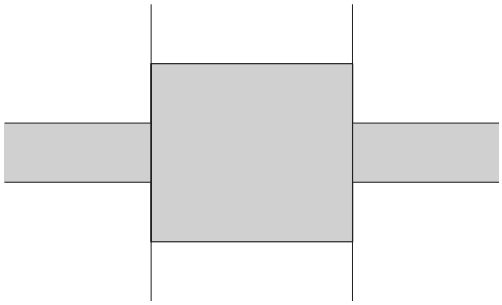

Figure 1. Example of a simple device with three sections and two interfaces.

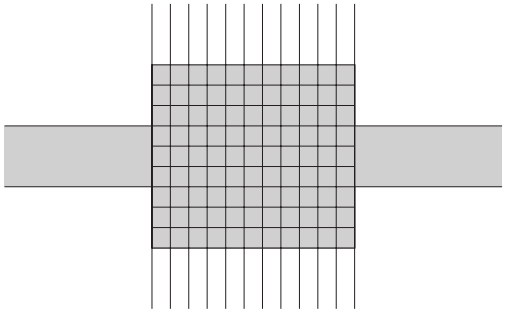

Figure 2. Example of a device where the middle section is considered nonlinear.

Different sections are connected with reflection and transmission matrices, constructed by the mode-matching algorithm that enforces continuity of the tangential electric and magnetic fields. Combining these matrices with the propagation matrices of a section, one constructs the entire scattering behavior of a device. Full-vectorial fields are assumed, and we note that this method is frequency domain.

An important point is the transversal boundaries. To model radiation losses in this direction one can use advanced PML (perfectly matched layer) boundary conditions. For the cylindrical multimode devices of section 3 we extended our framework so that different sections can have different radii. This proved to be efficient to gather the reflection coefficients of very confined modes to 'open' space. We mention that in this algorithm there is no need for longitudinal boundaries. For more information we refer to Ref. 1. This method is implemented in the CAMFR software package, which is freely available at http://camfr.sf.net.

2.2 Nonlinear devices

We have extended the eigenmode modeling framework for the Kerr effect[2] and for second-harmonic generation.[3] In this Proceeding we only discuss the Kerr extension. The Kerr effect is a third-order nonlinearity; it means that the refractive index is dependent on the local intensity of the electric field. To model this we include a grid for the nonlinear sections, and we apply an iterative approach. We perform a series of *linear* calculations. At each iteration the refractive index is updated through the Kerr nonlinear relation. After a number of iterations the field converges onto the full nonlinear solution.

This method is useful if the nonlinear sections are not too large. Therefore, the method is very suitable for localized resonances such as photonic crystal defect cavities, see section 4. In these cases only the defects need to be considered nonlinear, as they have the strongest fields. In this way the sections before and after the cavities need to be calculated only once, as their scattering matrix is power independent. Similar cavity systems are therefore simulated in seconds or minutes.

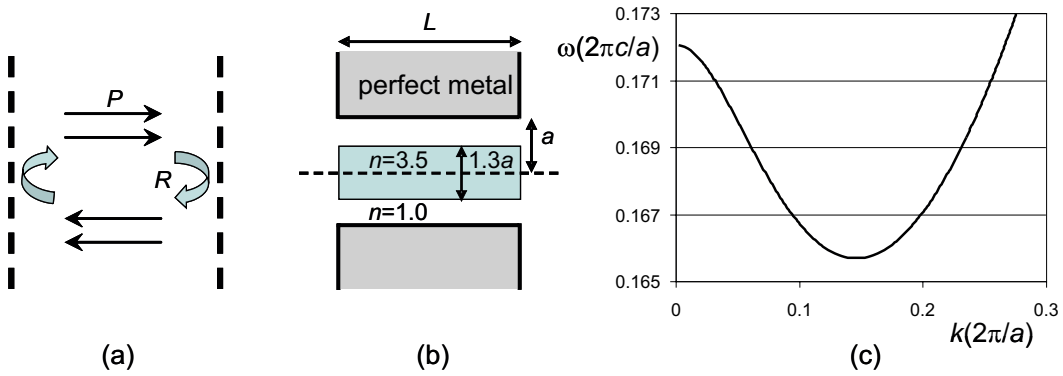

Figure 3. (a) Sketch of the modes interacting inside the cavity. (b) Depiction of the cylindrical geometry. (c) Dispersion of the central waveguide.

3. MULTIMODE CAVITIES

Guided by mode expansion calculations we have constructed a detailed description of a class of high quality cavities. The cavity itself consists of a waveguide with two (or more) guided modes. At certain lengths and frequencies the transmissions of the two modes at a facet interfere destructively, leading to low loss resonators. The mechanism of multipole cancelation[4] is evident in the far-field. The particular resonance parameters are elucidated by a semi-analytical model, described in the next subsection. An important factor for these resonances seems to be a strong coupling between the modes. This emerges for example in the context of zero group velocity modes. The current work therefore provides a more in-depth view of the modes described in Ref. 5.

3.1 Semi-analytical description

The class of devices we discuss is quite general. The devices consist of a section of waveguide with two guided modes. In that case the behavior of the cavity modes is very well described by the dispersion of the waveguide modes and their reflection properties at the facets. A sketch of the situation is shown in Fig. 3(a). Propagation is described by the propagation matrix

$$P = \begin{bmatrix} \exp(-ik_0 L) & 0 \\ 0 & \exp(-ik_1 L) \end{bmatrix}. \tag{1}$$

Here, k_0 and k_1 are the propagation constants of the guided waveguide modes, and L is the cavity length. The interaction of the modes at the facet is given by the complex elements of the reflection matrix

$$R = \begin{bmatrix} r_{00} & r_{01} \\ r_{10} & r_{11} \end{bmatrix}, \tag{2}$$

where, because of reciprocity, $r_{01} = r_{10}$. For convenience we often work with $k_0 = k + \Delta, k_1 = k - \Delta$ and $r_{00} = d + \delta, r_{11} = d - \delta$.

As usual, a cavity mode is achieved if the imaginary part of an eigenvalue of the round-trip matrix (or, because of symmetry, half-trip matrix) is zero. The half-trip matrix is given by $P \times R$. In case of resonance, the quality factor Q of the cavity mode is determined by the magnitude of its eigenvalue, or, more precisely, by how close the half-trip eigenvalue is to ± 1. One obtains

$$Q = \frac{\omega_r L}{|v_g|\,(1 - |\lambda|^2)}. \tag{3}$$

Here, ω_r is the resonance frequency of the cavity mode and L is the length of the waveguide. v_g is the group velocity of the waveguide modes. (The formula can be extended in case of different group velocities.) λ is the

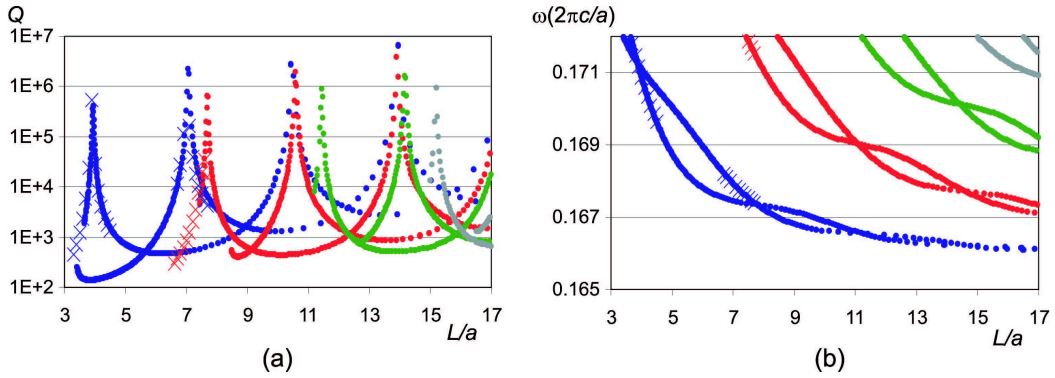

Figure 4. (a) Q versus L of the resonances. Dots are data points from mode expansion (CAMFR), crosses present results from FDTD (MEEP). (b) ω versus L for the same cavity modes.

eigenvalue of the half-trip matrix, so

$$P \times R \begin{bmatrix} c_0 \\ c_1 \end{bmatrix} = \lambda \begin{bmatrix} c_0 \\ c_1 \end{bmatrix}, \tag{4}$$

with c_0 and c_1 the complex eigenvector components corresponding with the eigenvalue λ. In the end, we get the following general formula for this eigenvalue

$$\lambda = \exp(-i\Delta L)\left[d\cos(kL) - i\delta\sin(kL) \pm \sqrt{(-id\sin(kL) + \delta\cos(kL))^2 + r_{01}^2}\right]. \tag{5}$$

If we obtain the propagation constants and reflection matrix elements by numerical means, this equation provides a very accurate description of the cavity modes. We obtain information such as lengths, frequencies and quality factors.

3.2 Example

The previous is applied to the device of Ref. 5. The geometry and parameters of the cylindrical cavity are shown in Fig. 3(b). There is free space to the left and to the right of the structure. The dispersion relation of the central waveguide is depicted in Fig. 3(c). We note that the appearance of the zero group velocity point creates two strongly interacting guided modes. A numerical sweep with eigenmode expansion over the lengths and frequencies uncovers an intricate cavity mode structure, see Fig. 4. In these figures a dot is added each time a resonance is found, thus each time the imaginary part of the eigenvalue becomes zero. Very high-quality resonances are uncovered, that are ordered along several branches. Different intertwined pairs correspond to different orders, and the crossing lines in a pair correspond to different symmetries (node versus antinode in the center of the cavity).

The far field distribution of the modes shows that the multipole cancelation effect is at work, as described in Ref. 4. At a high-Q resonance the radiation pattern changes: there are extra nodal lines, as the lowest order multipole is canceled. This gives proof of a bimodal mechanism: Both waveguide modes are prominent in the cavity. At the facets they reflect but radiate some energy into the space adjacent to the cavity. This radiation can be described as a superposition of multipoles. At certain cavity lengths and frequencies two conditions are fulfilled: there is a phase resonance (imaginary part of λ is zero), and the important lowest order multipole contribution of the modes cancel each other (leading to a real part of λ close to one, meaning low losses). When these conditions are satisfied we obtain a high-quality cavity. This mechanism was also at work in the two-dimensional square structures of Ref. 6 and Ref. 7.

Eq. 5 also gives us more information about the position of these resonances. It turns out that in many cases one can approximate by inspecting the reflection matrix. For the current example this data is shown in Fig. 5. For a large range of frequencies it is clear that the off-diagonal element is larger than the diagonal ones, thus

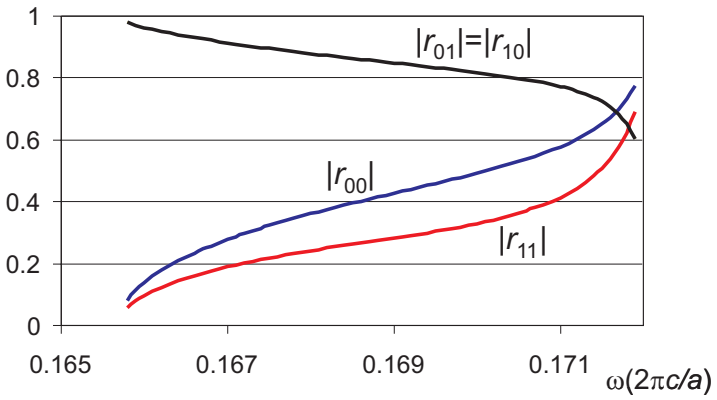

Figure 5. Magnitudes of the reflection matrix elements for the cylindrical structure.

$|r_{01}| > |r_{00}|, |r_{11}|$ (or $|r_{01}| > |d|, |\delta|$). In that case the magnitude of the eigenvalues (from Eq. 5) is approximated by:

$$|\lambda|^2 \approx |r_{01}|^2 \pm 2\cos(kL)\mathrm{Re}(r_{01}d^*) \mp 2\sin(kL)\mathrm{Im}(r_{01}\delta^*), \tag{6}$$

where Re (Im) is the real (imaginary) part, and * means complex conjugate. This expression implies that the magnitude of λ (at constant L) is only a weakly-varying function of the frequency. In function of L (at constant ω) the maxima of $|\lambda|^2$ are separated by π/k or $3.4a$. Note that in this example k corresponds with the zero v_g-point. This indicates that the quality factor extrema for different orders should happen around this length scale, this is clearly visible in Fig. 4(a). A similar approximation is possible to discuss the phase of the eigenvalue. In this way one gains insight into the trends of Fig. 4(b).

We have examined this mechanism in other settings. For example when both modes have a positive group velocity, or in a plasmonic waveguide. The portraits, as in Fig. 4, have different trends, which are explained by different propagation constants and reflection matrices. However, the mechanism of multipole or mode cancelation remains the same, and it is accurately described by the previous methods. For a description of these examples we refer to Ref. 8.

4. NONLINEAR CAVITIES

An example of a photonic crystal structure where two cavities are interacting through a connecting waveguide is shown in Fig. 6(b). It is well known that the cascading of resonators gives rise to new filter functions. However, the case of coupled *nonlinear* cavities is less studied.[9]

In the current device we explore the situation when the input powers into the waveguide from both sides are equal. In the linear case this will always give equal output powers to the left and to the right. In the nonlinear case, however, this symmetric solution can become unstable, and a symmetry breaking instability ensues. This effect arises because of nonlinear feedback effects between the resonators. For the asymmetric case there are two corresponding solutions: more power exits to the right than to the left, and vice versa. It turns out one can switch between these states by employing pulses. Thus, one obtains a flip-flop behavior.

4.1 Coupled-mode theory

The numerical simulations agree very well with the coupled-mode theory. Furthermore, this theory allows for a very efficient exploration of the parameter space, even in the time-domain. In addition, it provides for an elegant description of the effect. A sketch of the amplitudes relevant for this theory is shown in Fig. 6(a). The structure is described by:[9]

$$\frac{\mathrm{d}a_j}{\mathrm{d}t} = \left[i\left(\omega_0 + \delta\omega_j\right) - \frac{1}{\tau}\right] a_j + df_j + db_{j+1}, \tag{7}$$

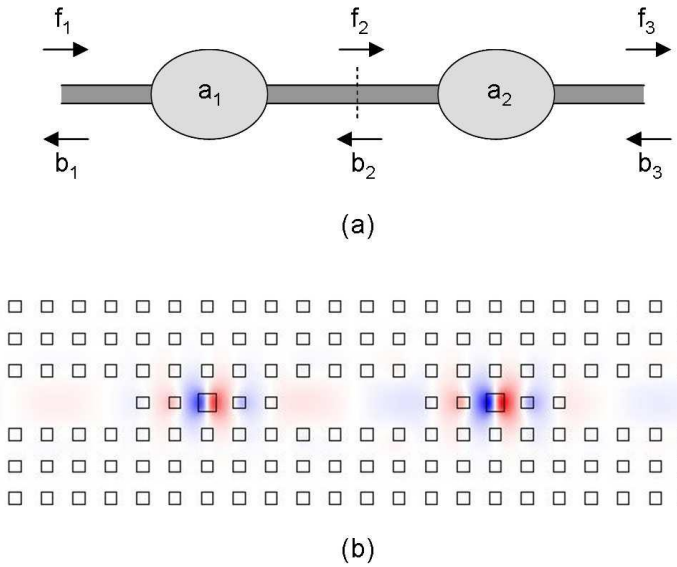

Figure 6. (a) Schematic of the coupled cavity structure. (b) The photonic crystal device, with 4 periods in between the switches. An electric field distribution is superimposed to illustrate the defect modes.

$$b_j = \exp(i\phi) f_j + d a_j, \tag{8}$$

$$f_{j+1} = \exp(i\phi) b_{j+1} + d a_j, \tag{9}$$

for $j = 1, 2$. Here $d = i\exp(i\phi/2)/\sqrt{\tau}$, where ϕ represents the phase that depends on the waveguide length and the photonic crystal reflection properties. The nonlinear frequency shift is $\delta\omega_j = -|a_j|^2/(P_0\tau^2)$, with P_0 the 'characteristic nonlinear power' of the cavity.[10] In these equations $|a_j|^2$ is the energy in the cavity mode. $|f_j|^2$ (resp. $|b_j|^2$) represents the power flowing in the (single-mode) waveguide in the forward (resp. backward) direction. Thus, $|f_1|^2 \equiv P_{in}^L$ (resp. $|b_3|^2 \equiv P_{in}^R$) is the input power from the left (resp. right), and $|b_1|^2 \equiv P_{out}^L$ (resp. $|f_3|^2 \equiv P_{out}^R$) is the output power to the left (resp. right).

We assume $f_1 = b_3$, thus equal input power (and phase) from both sides. After some manipulation of the coupled mode equations we get:[11]

$$(A - B)\left[(A^2 + AB + B^2) + 2\Delta'(A + B) + \Delta'^2 + 1/4\right] = 0, \tag{10}$$

with dimensionless cavity energies $A = \alpha|a_1|^2$ and $B = \alpha|a_2|^2$, where $\alpha = -1/(P_0\tau)$. Furthermore, the detuning $\Delta' = \Delta + \tan(\phi/2)/2$, with $\Delta = \tau(\omega_0 - \omega)$. From Eq. 10 we learn that there is the possibility of an asymmetric solution $A \neq B$, apart from the symmetric solution $A = B$. The asymmetric solution appears (for certain input powers) if the detuning Δ' is chosen correctly, and if the solution is stable. From Eq. 10 it is straightforward to derive a criterion: The asymmetric solution exists if $|\Delta'| > \sqrt{3}/2$. Furthermore, stability analysis (not presented here) shows that the symmetric solution destabilizes into the asymmetric solutions.

4.2 Switching

The appearance of symmetry breaking solutions is shown by rigorous eigenmode calculations and coupled mode theory. Fig. 7 presents the output versus input characteristics in two cases. For some parameters it is possible to obtain zero output in one direction, which provides a high contrast.

The next step is to study how one can switch between the different asymmetric states. It turns out that it is possible to change from one state to the other by applying pulses at the correct input. So one can flip e.g. from the case where the right output power is larger than the left, to the case where the left output is larger.

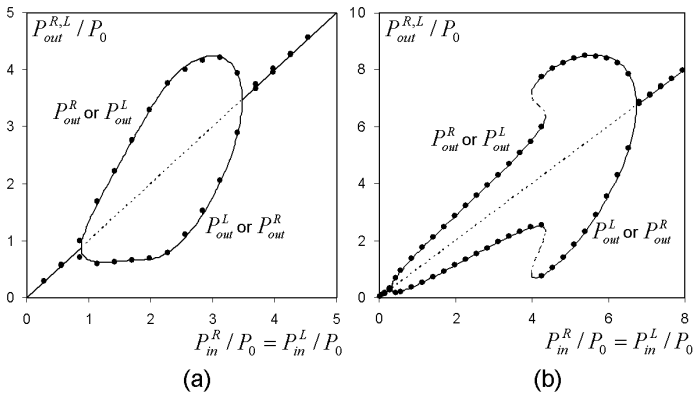

Figure 7. Output power versus input power for (a) $\Delta = 1.039$, $\phi = 0.570$ and (b) $\Delta = 2.0$, $\phi = 0.595$. Stable and unstable states obtained with coupled mode theory are shown with solid and dashed lines, respectively. Dots show rigorous simulation results.

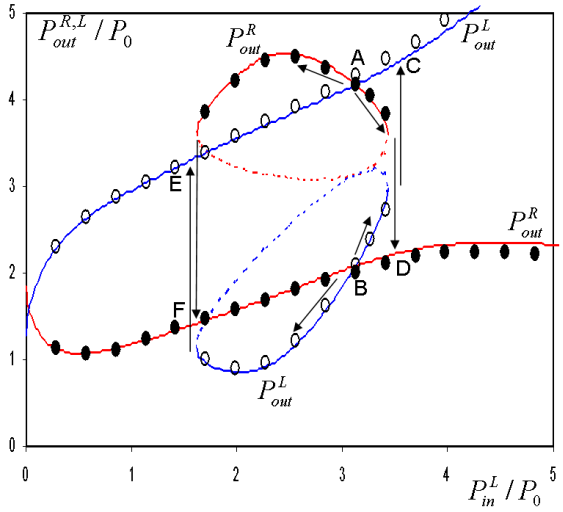

Figure 8. Output powers versus left input power P_{in}^{L} at $\Delta = 1.039$, $\phi = 0.570$ and $P_{in}^{R} = 3.125P_0$. Stable states for P_{out}^{R} (resp. P_{out}^{L}) are shown with red (resp. blue) solid lines. Dashed lines indicate unstable states. Dots (resp. circles) show rigorous simulation results for P_{out}^{R} (resp. P_{out}^{L}). Labels AB, CD and EF display key states.

This switching can be shown both in the frequency and the time domain. The results for the frequency domain are seen in Fig. 8. Here the input power from the right P_{in}^{R} is held constant, while the one from the left P_{in}^{L} is varied. Starting from state AB, in the situation where $P_{out}^{R} > P_{out}^{L}$, we follow the arrows to the right, if we increase P_{in}^{L}. Eventually this branch stops and we flip to state CD, with $P_{out}^{R} < P_{out}^{L}$. Decreasing P_{in}^{L} we again reach state AB, but now the outputs are flipped. We could also follow the arrows to the left, by decreasing P_{in}^{L}, starting from state AB, again with $P_{out}^{R} > P_{out}^{L}$. Then we reach the left end of the branch, and the solution jumps to the state EF, with $P_{out}^{R} < P_{out}^{L}$. Increasing P_{in}^{L} brings the system to the flipped state AB. Once the system is flipped, one needs to add or remove power at the other side to flip again. This corresponds to changing the left/right labels L and R in Fig. 8.

The coupled mode equations can also be applied to study the time domain behavior. In this way we have confirmed switching in time.[11] In experiments the cavities are not identical. We have checked the case where

the resonance frequencies differ, say one has ω_0^A and ω_0^B. The solutions are more complex (the states become non-degenerate). However, the functionality remains the same, up until a certain resonance frequency difference. This tolerance depends upon the detuning. With the parameters of Fig. 7(b), a non-optimized value for the tolerance amounts to $|\omega_0^A - \omega_0^B|/\omega_{avg} < 0.5/Q$, with $\omega_{avg} = (\omega_0^A + \omega_0^B)/2$.

In addition, we examined the case where the cavities are next to the waveguide,[9] instead of in the waveguide. Similar symmetry breaking phenomena appear, and the same methods are applicable.

5. CONCLUSIONS

We have shown that eigenmode expansion calculations are useful for a wide range of devices. Both the linear and Kerr nonlinear algorithms are reviewed. As a concrete linear example we examine a class of high-quality multimode cavities. Here, the mechanism is interference between two guided modes inside the cavity, leading to mode or multipole cancelation outside of the resonator. For the nonlinear extension we present symmetry breaking phenomena in coupled photonic crystal resonators. The nonlinear feedback effects create opportunities for all-optical flip-flop devices. In both cases the rigorous numerical treatment is confirmed and enhanced by a semi-analytical description.

ACKNOWLEDGMENTS

BM and PB acknowledge postdoctoral fellowships from the Funds for Scientific Research - Flanders (FWO-Vlaanderen). We acknowledge the Belgian DWTC project IAP-Photon and the NSF MRSEC grant DMR-02-13282.

REFERENCES

1. P. Bienstman and R. Baets, "Optical modelling of photonic crystals and VCSELs using eigenmode expansion and perfectly matched layers," Opt. Quantum Electron. **33,** 327–341 (2001).
2. B. Maes, P. Bienstman, and R. Baets, "Modeling of Kerr nonlinear photonic components with mode expansion," Opt. Quantum Electron. **36,** 15–24 (2004).
3. B. Maes, P. Bienstman, and R. Baets, "Modeling second-harmonic generation by use of mode expansion," J. Opt. Soc. Am. B **22,** 1378–1383 (2005).
4. S.G. Johnson, S. Fan, A. Mekis, and J.D. Joannopoulos, "Multipole-cancellation mechanism for high-Q cavities in the absence of a complete photonic band gap," Appl. Phys. Lett. **78,** 3388–3390 (2001).
5. M. Ibanescu, S.G. Johnson, D. Roundy, Y. Fink, and J.D. Joannopoulos, "Microcavity confinement based on an anomalous zero group-velocity waveguide mode," Opt. Lett. **30,** 552–554 (2005).
6. M. Hammer, "Resonant coupling of dielectric optical waveguides via rectangular microcavities: the coupled guided mode perspective," Opt. Comm. **214,** 155–170 (2002).
7. M. Hammer, "Total multimode reflection at facets of planar high-contrast optical waveguides," Journ. Lightw. Tech. **20,** 1549–1555 (2002).
8. B. Maes, M. Ibanescu, J.D. Joannopoulos, P. Bienstman, and R. Baets, "Microcavities based on multimodal interference," Opt. Exp. **15,** 6268–6278 (2007).
9. B. Maes, P. Bienstman, and R. Baets, "Switching in coupled nonlinear photonic-crystal resonators," J. Opt. Soc. Am. B **22,** 1778–1784 (2005).
10. M. Soljačić, M. Ibanescu, S.G. Johnson, Y. Fink, and J.D. Joannopoulos, "Optimal bistable switching in nonlinear photonic crystals," Phys. Rev. E **66,** 055601(R) (2002).
11. B. Maes, M. Soljačić, J.D. Joannopoulos, P. Bienstman, R. Baets, S.-P. Gorza, and M. Haelterman, "Switching through symmetry breaking in coupled nonlinear micro-cavities," Opt. Exp. **14,** 10678–10683 (2006).

PROCEEDINGS OF SPIE

Photonics North 2007

John Armitage
Editor

4–7 June 2007
Ottawa, Ontario, Canada

Organized by
Canadian Photonics Consortium (Canada)
Ottawa Photonics Cluster (Canada)
Quebec Photonic Network (Canada)
Carleton University (Canada)
University of Ottawa (Canada)

Sponsored by
Oz Optics Ltd. (Canada)
Ontario Centres of Excellence (Canada)

Cosponsored by
Optoelectronics Industry Development Association (Canada)
OPIN—Ontario Photonics Industry Network (Canada)

Cooperating Organization
SPIE

Published by
SPIE

Part One of Two Parts

Volume 6796

Proceedings of SPIE, 0277-786X, v. 6796

The papers included in this volume were part of the technical conference cited on the cover and title page. Papers were selected and subject to review by the editors and conference program committee. Some conference presentations may not be available for publication. The papers published in these proceedings reflect the work and thoughts of the authors and are published herein as submitted. The publisher is not responsible for the validity of the information or for any outcomes resulting from reliance thereon.

Please use the following format to cite material from this book:
Author(s), "Title of Paper," in *Photonics North 2007*, edited by John Armitage, Proceedings of SPIE Vol. 6796 (SPIE, Bellingham, WA, 2007) Article CID Number.

ISSN 0277-786X
ISBN 9780819469625

Published by
SPIE
P.O. Box 10, Bellingham, Washington 98227-0010 USA
Telephone +1 360 676 3290 (Pacific Time) · Fax +1 360 647 1445
SPIE.org

Printed in the United States of America.

Publication of record for individual papers is online in the SPIE Digital Library.

SPIEDigitalLibrary.org

Paper Numbering: Proceedings of SPIE follow an e-First publication model, with papers published first online and then in print and on CD-ROM. Papers are published as they are submitted and meet publication criteria. A unique, consistent, permanent citation identifier (CID) number is assigned to each article at the time of the first publication. Utilization of CIDs allows articles to be fully citable as soon they are published online, and connects the same identifier to all online, print, and electronic versions of the publication. SPIE uses a six-digit CID article numbering system in which:

- The first four digits correspond to the SPIE volume number.
- The last two digits indicate publication order within the volume using a Base 36 numbering system employing both numerals and letters. These two-number sets start with 00, 01, 02, 03, 04, 05, 06, 07, 08, 09, 0A, 0B … 0Z, followed by 10-1Z, 20-2Z, etc.

The CID number appears on each page of the manuscript. The complete citation is used on the first page, and an abbreviated version on subsequent pages. Numbers in the index correspond to the last two digits of the six-digit CID number.